Virgo cluster and field dwarf ellipticals in 3D - III. Spatially and temporally resolved stellar populations

Ryś, Agnieszka; Koleva, Mina; Falcón-Barroso, Jesús; Vazdekis, Alexandre; Lisker, Thorsten; Peletier, Reynier; van de Ven, Glenn

Published in:
Monthly Notices of the Royal Astronomical Society

DOI:
10.1093/mnras/stv1364

Monthly Notices of the ROYAL ASTRONOMICAL SOCIETY

MNRAS **452,** 1888–1901 (2015) doi:10.1093/mnras/stv1364

Virgo cluster and field dwarf ellipticals in 3D – III. Spatially and temporally resolved stellar populations

Agnieszka Ryś,[1,2]★ Mina Koleva,[3] Jesús Falcón-Barroso,[2,4] Alexandre Vazdekis,[2,4] Thorsten Lisker,[5] Reynier Peletier[6] and Glenn van de Ven[7]

[1] *European Southern Observatory, Karl-Schwarzschild-Strasse 2, D-85748 Garching bei Muenchen, Germany*
[2] *Instituto de AstrofÃsica de Canarias, Vía Láctea s/n, E-38205 La Laguna, Tenerife, Spain*
[3] *Sterrenkundig Observatorium, Ghent University, Krijgslaan 281, S9, B-9000 Gent, Belgium*
[4] *Departamento de Astrofísica, Universidad de La Laguna, E-38205 La Laguna, Tenerife, Spain*
[5] *Astronomisches Rechen-Institut, Zentrum für Astronomie der Universität Heidelberg, Mönchhofstrasse 12-14, D-69120 Heidelberg, Germany*
[6] *Kapteyn Astronomical Institute, University of Groningen, Postbus 800, NL-9700 AV Groningen, the Netherlands*
[7] *Max Planck Institute for Astronomy, Königstuhl 17, D-69117 Heidelberg, Germany*

Accepted 2015 June 17. Received 2015 June 8; in original form 2015 March 23

ABSTRACT

We present the stellar population analysis of a sample of 12 dwarf elliptical galaxies, observed with the SAURON integral field unit, using the full-spectrum fitting method. We show that star formation histories (SFHs) resolved into two populations can be recovered even within a limited wavelength range, provided that high signal-to-noise ratio (S/N) data are used. We confirm that dEs have had complex SFHs, with star formation extending to (more) recent epochs: for the majority of our galaxies star formation activity was either still strong a few ($\lesssim$5) Gyr ago or they experienced a secondary burst of star formation roughly at that time. This latter possibility is in agreement with the proposed dE formation scenario where tidal harassment drives the gas remaining in their progenitors inwards and induces a star formation episode. For one of our field galaxies, ID 0918, we find a correlation between its stellar population and kinematic properties, pointing to a possible merger origin of its kinematically decoupled core. One of our cluster objects, VCC 1431, appears to be composed exclusively of an old population ($\gtrsim$10–12 Gyr). Combining this with our earlier dynamical results, we conclude that the galaxy was either ram-pressure stripped early on in its evolution in a group environment and subsequently tidally heated, or that it evolved *in situ* in the cluster's central parts, compact enough to avoid tidal disruption. These are only two of the examples illustrating the SFH richness of these objects confirmed with our data.

Key words: galaxies: dwarf – galaxies: evolution – galaxies: formation – galaxies: structure.

1 INTRODUCTION

Dwarf elliptical galaxies (dEs) have, as a class, received a significant amount of attention in the literature in recent years. This is because with the advent of higher resolution/more sensitive instruments it became feasible to study these low-surface-brightness systems in more detail. A great deal of complexity of their structure has been revealed, prompting some works to introduce a complex classification system and sometimes view the different subclasses as intrinsically distinct populations. We know that their photometry shows underlying structures such as spiral arms (e.g. Jerjen, Kalnajs & Binggeli 2000), bars, and discs (e.g. Lisker, Grebel & Binggeli 2006a). A similar variety was found in their kinematic and stellar population properties. We know of Virgo and field dEs harbouring kinematically decoupled cores (KDC; e.g. De Rijcke et al. 2004; Geha, Guhathakurta & van der Marel 2005; Ryś, Falcón-Barroso & van de Ven 2013; Toloba et al. 2014; Guerou et al. 2015). dE stellar populations show indications of both young and old ages and varied gradients (e.g. Koleva et al. 2009b; Koleva et al. 2011; Ryś & Falcón-Barroso 2012).

Recent evidence has caused the majority of literature to favour the environmental transformation scenario for dEs, where their progenitors are assumed to be late-type galaxies that were transformed once they entered the denser (cluster) environment (e.g. Geha et al. 2010; Janz et al. 2012; Kormendy & Bender 2012; Toloba et al. 2012; Lisker et al. 2013; Ryś et al. 2013). The notion was, in fact, first proposed as early as 1944 by Baade based on his study of

★ E-mail: arys@eso.org

Local Group (LG) dEs NGC 185 and NGC 147. The claim reappeared later in the works of Kormendy (1985), Binggeli, Sandage & Tammann (1988), Binggeli & Cameron (1991) and Bender, Burstein & Faber (1992). A few mechanisms have been proposed that may be responsible for such environmentally induced transformation. Ram-pressure stripping (Gunn & Gott 1972; Lin & Faber 1983) can remove a galaxy's remaining gas reservoir on relatively short time-scales so that the star formation (SF) stops quickly once the galaxy enters denser environments. It has been directly shown for massive spiral galaxies in Virgo in Chung et al. (2007). In the galaxy harassment scenario (Moore, Lake & Katz 1998), the tidal interactions between the galaxy and the intergalactic medium (or in the extreme cases, galaxy–galaxy interactions) can heat up the object and slow its rotation down (albeit not remove it completely). They are also able to remove both stellar and, more strongly, dark mass.

Finding the progenitors of dEs is not a straightforward task. First of all because what we look at today are *present-day analogues of the presumed late-type progenitors* of dEs. Thus, none of the late-type galaxy types considered to be progenitor candidates for dEs (e.g. dIrrs, dwarf spirals) can really play that role. They have evolved in parallel, albeit evidently under different circumstances. This was first pointed out by Binggeli (1994) and Skillman & Bender (1995) and repeated more recently in, e.g. Lisker et al. (2013) who also added that the conditions a few Gyr ago were necessarily different, in terms of density distribution and so the interactions between galaxies and between galaxies and the surrounding medium did not resemble those we see today.

In observational studies only general statements are typically made about certain scenarios being compatible (or not) with a given observational result. Few attempts have been made at a quantitative discrimination between the processes because this requires making a priori assumptions about the progenitors. We have faced a similar challenge in the interpretation of our previous work. In Ryś et al. (2013) (Paper I of our series), the variety of properties we discuss there could be due to either stochastic environmental processes or the fact that the progenitor family consists of galaxies of various types. Later in Ryś, van de Ven & Falcón-Barroso (2014, hereafter Paper II), we compared the dynamical properties of our dEs to those of dwarf and giant late-type objects and we concluded that a transformation mechanism is required which not only is able to lower the angular momentum but also needs to account for the increased stellar concentration of dEs with respect to their presumed progenitors. This could be achieved either in the case of harassment being the important mechanism, or it could be explained by assuming that the progenitors were already more compact at higher redshift. While these findings have naturally narrowed down the range of possibilities for the formation paths, a number of open questions still remained.

Here (Paper III of the series) we investigate the star formation histories (SFHs) of our sample using the full-spectrum fitting technique, with the view to further narrowing down the above results. The paper is structured as follows. A summary of the sample selection, observations, and data reduction is presented in Section 2. In Section 3 we describe the methods used in the analysis. Section 4 presents our results which are then discussed in Section 5. The findings are summarized in Section 6.

2 DATA

Details on data selection, observations and data reduction are presented in Ryś et al. (2013). In short, we observed 12 dEs: nine in the Virgo Cluster and three in the field (see Table 1 for their basic properties). Our objects span a wide range of ellipticities and distances from the cluster's centre. The observations were carried out in 2010 Jan and 2011 Apr (eight nights in total) using the WHT/SAURON instrument at the Roque de los Muchachos Observatory in La Palma, with each galaxy typically exposed for 5 h. For the extraction and calibration of the data we followed the procedures described in Bacon et al. (2001) using the specifically designed XSAURON software developed at the Centre de Recherche Astrophysique de Lyon (CRAL). We filtered out all individual spaxels with signal-to-noise ratio (S/N) <7 which roughly corresponds to surface brightness of $\mu_V \approx 23.5$ mag at the edge of the fields (slightly depending on the object).[1] In the original analysis presented in Papers I and II the data were spatially binned to achieve the minimum S/N of 30. Here we binned the data in annuli of increasing width so as to achieve yet higher S/N. Also, the properties derived in such a way are not biased towards any particular galaxy axis which presents an advantage over the traditionally employed long-slit data. It is also important to stress the full or nearly full 2D spatial coverage of our data: for the shown radial extent the coverage is $\gtrsim$95 per cent for all galaxies and annuli, with only one exception of the outermost annulus of VCC 0929 (∼70 per cent).

Fig. 1 shows an example of a central spectrum of one of the galaxies, collapsed within an aperture with a 3-arcsec diameter, used in the Sloan Digital Sky Survey (SDSS)/SAURON comparison presented in Section 4.

Table 1. Observed objects: name, distance (for the Virgo objects from Mei et al. 2007 where available, otherwise 17 Mpc assumed), morphological type (from Lisker et al. 2007), ellipticity, *r*-band effective radius, and *r*-band apparent magnitude. Adapted from Ryś et al. (2013).

Object	Distance (Mpc)	Type	ϵ	R_e (arcsec)	m_r (mag)
VCC 0308	17.00	dE(di;bc)	0.07	18.7	13.32
VCC 0523	16.74	dE(di)	0.29	27.9	12.60
VCC 0929	17.00	dE(N)	0.11	22.1	12.65
VCC 1036	17.00	dE(di)	0.56	17.2	13.13
VCC 1087	16.67	dE(N)	0.31	28.6	12.85
VCC 1261	18.11	dE(N)	0.42	19.7	12.87
VCC 1431	17.00	dE(N)	0.03	9.6	13.60
VCC 1861	16.14	dE(N)	0.01	20.1	13.41
VCC 2048	17.00	dE(di)	0.48	16.5	13.08
NGC 3073	17.8	dE/dS0	0.15	16.1	12.98
ID 0650	25.9	dE/S0	0.10	20.1	13.73
ID 0918	16.3	dE/E	0.27	6.4	13.79

3 METHODS

To derive SFHs of our galaxies we use the full-spectrum fitting package ULySS of Koleva et al. (2009b). In ULySS, an observed spectrum is fitted against a model expressed as a linear combination of non-linear components [a function of age, [Fe/H], and [Mg/Fe]), returning the spectrum of a single stellar population], optionally convolved with a line-of-sight velocity distribution (LOSVD) and multiplied by a polynomial function, meant to absorb errors in, e.g.

[1] By filtering out low-S/N spaxels we made sure that our final binned spectra were not contaminated by low-quality measurements. Simply adding up the signal of individual spaxels to form larger bins will lead to lower overall S/N if some of the input spaxels have low S/N, and, in our case, showed as a spread of σ values that exceeded the nominal measurement errors.

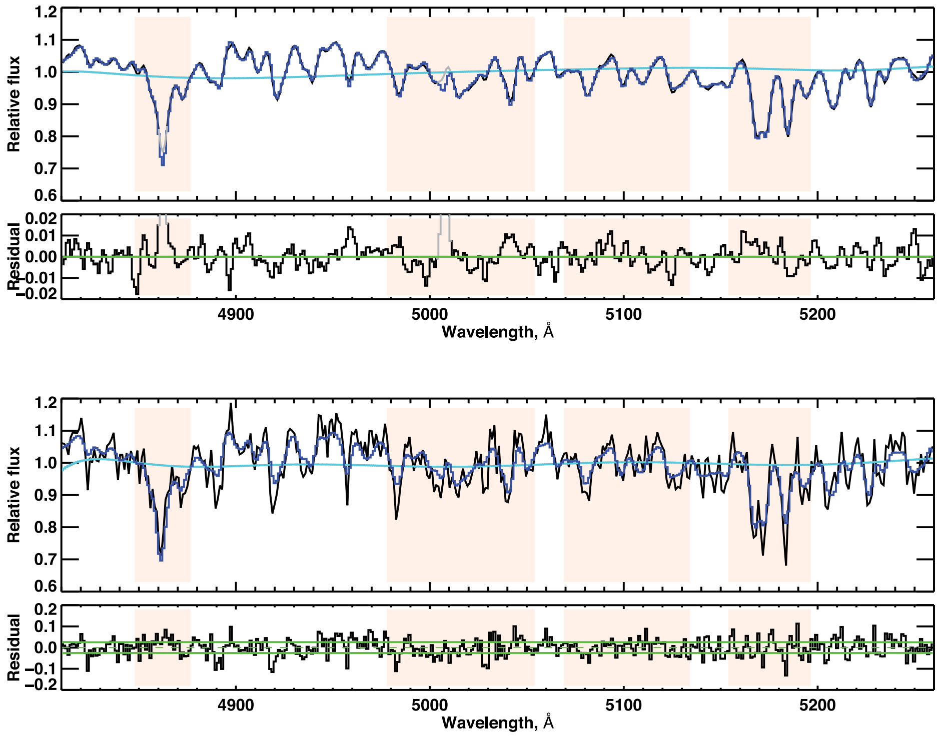

Figure 1. Example ULySS fits to the VCC 0523 galaxy central spectrum (collapsed within an aperture with a 3-arcsec diameter) for our SAURON data (upper panel) and SDSS data (lower panel), shown here for the SAURON wavelength range. The ordinate values are plotted on normalized scales. The S/N of the SAURON spectra exceeds 100 per pixel. The data are shown with black lines, models – blue lines, and the masked pixels are in grey. The light blue line is the multiplicative polynomial used in the fit. The regions of Lick indices are shaded in light pink. In the small panels below the spectrum we plot the residuals between the data and the model, shown as a percentage of the original value (note that in the case of SDSS the *y*-range of the bottom panels is 10 times larger than that for the SAURON spectra).

flux calibration [for details on ULySS see Koleva et al. (2009b) sections 2 and 4]. As reference models we use the extended MILES models (Vazdekis et al. 2010; Vazdekis et al. 2012) and Pegase.HR (Le Borgne et al. 2004).

We first compared SFHs extracted from the archival SDSS and our SAURON data. To this end, for each SAURON galaxy in common with SDSS spectroscopic data (10 objects) we extracted spectra collapsed within an aperture with a 3-arcsec diameter (see Fig. 1 for an example). We then compared the recovered SFHs coming from the following data sets (Fig. 2):

(i) original SDSS,
(ii) SDSS restricted to SAURON wavelength range,
(iii) SAURON.

The idea behind the approach was to test how/if restricting available wavelength range influences the accuracy of recovered SFHs and whether or not it is possible to compensate for a limited wavelength range with high S/N.

To produce the SFHs we use 2-SSP fits. We have found this to be the best decomposition given our data constraints. 1-SSP fits can be viewed as a first-order approach to the true SFHs, but going one step further with 2-SSP decompositions we are in the position to address the science questions that have driven our analysis. To determine the best strategy we first produced 20-SSP fits where individual population parameters were not allowed to change. From the non-zero weighs of these 20 SSPs we concluded that we can reconstruct the history in two episodes, except for NGC 3073, for which we found that applying a three-burst decomposition provided the most reliable recovered SF parameters.

Then, using the MILES models (Vazdekis et al. 2012) we looked for a two-burst decomposition in the age ranges [100, 5000] Myr and [5000, 17 000] Myr. We found that many of the galaxies hit the age limit in particular the 100 Myr and the maximum Z of 0.2 dex. We therefore tried to use Pegase.HR/ELODIE3.1 (Prugniel & Soubiran 2001; Le Borgne et al. 2004) which goes to 10 Myr and metallicities of 0.69 (due to the different set of isochrones).[2] This was more successful as some of the galaxies found their best young population fits around 50 Myr, so using ELODIE we made sure that the model parameters were fully enclosed within the model grid.

In our subsequent reconstructions the ages of old populations were either left free or were fixed to 12 Gyr. Young populations' ages were left free in both cases. The metallicities were in each case left free within the limits of the models. When fitting, we have included SSPs together with Hβ, [O III 4959] and [O III 5007] lines in emission. We note, however, that significant emission was only detected in one of our field objects, NGC 3073. See also Ryś et al. (2013) for more details.

For those of the galaxies for which the program turned out to have difficulty finding an old population (VCC 0523, VCC 1087, VCC 1261, VCC 1861, VCC 2048, and ID 0650), we imposed more constraints by fixing the age of the old burst to 12 Gyr. The decision was motivated by the fact that old populations have so far been found in all studied dwarfs, not only in a comparable mass range

[2] As both the libraries are empirical, a full coverage of parameter space is not possible, therefore the quoted limits are reached through extrapolations performed with the use of theoretical libraries.

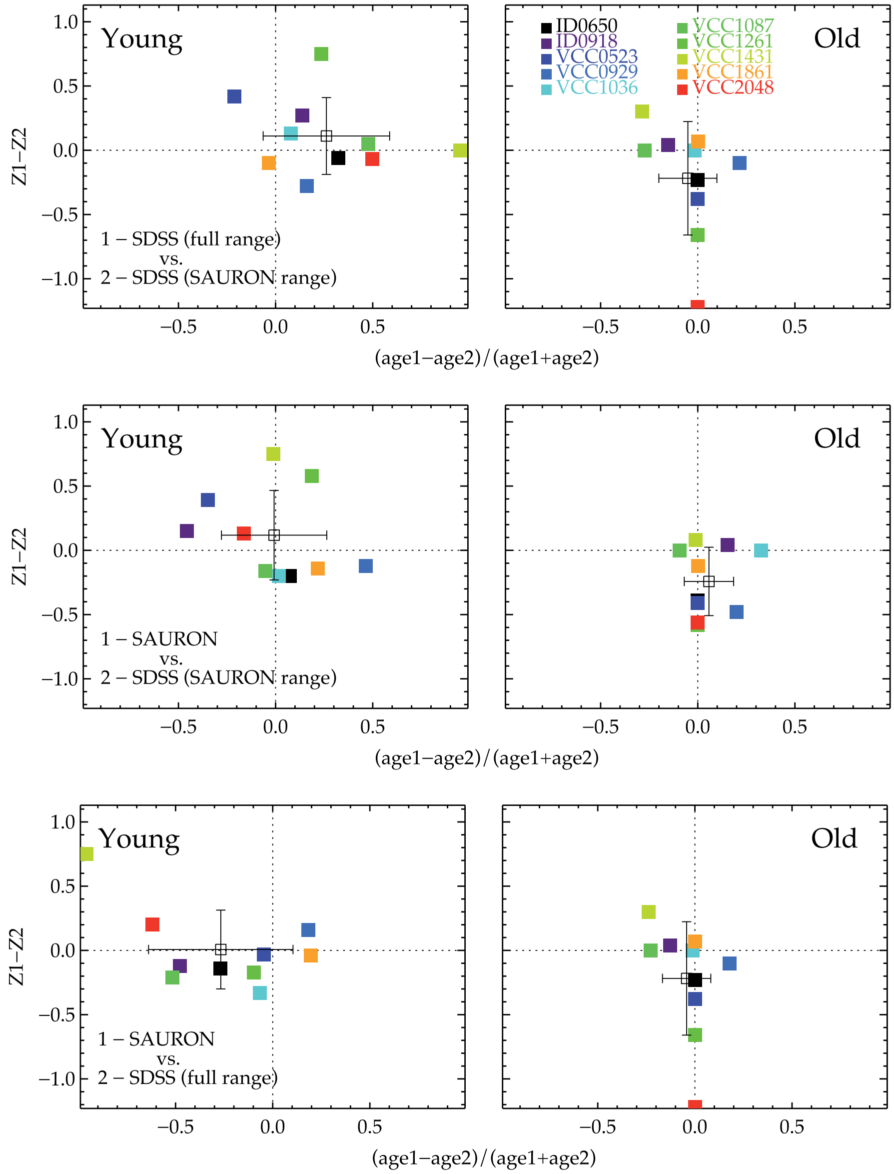

Figure 2. Comparison of the properties of young and old populations (ages, metallicities, and population weights from the following data sets): (1) SDSS – full wavelength range, (2) SDSS – wavelength range cut to the range of SAURON, (3) central 3 arcsec of our SAURON data. The *x*-axes show relative differences in age, and the *y*-axes show direct differences in metallicity (Z). The dotted lines indicate where the agreement between the data sets would be perfect. The open black symbols show average values of (Z1−Z2) and (age1−age2)/(age1+age2), with the error bars indicating standard deviations. All individual errors are shown in Table 2, which also includes population weights.

(e.g. Koleva et al. 2009b, 2011) but also in all dwarf early types and the vast majority (possibly all) of late- and transition-type dwarfs of the LG (Tolstoy, Hill & Tosi 2009). The difficulty, thus, most likely stems from the strong presence of younger populations, rather than a genuine lack of old stars.

The mass weight contained in each annulus comes from the fraction of each component used to obtain the best fit. Each of the SSPs is multiplied by this fraction and later the SSPs are summed to produce the best matching template. In Fig. 3 we show the relative contribution of each component, i.e. the weight of each SSP is normalized to the total weight.

As a consistency check, we have also compared our ULySS-based light-weighted ages and metallicites with those coming from the line-strength (LS) analysis which will be presented in our forthcoming paper (Ryś et al., in preparation). The comparison plots and their description are given in Appendix A. Overall, the values derived using the two methods agree to within the errors.

The SFHs for all galaxies and radial bins, including errors on the recovered parameters coming from Monte Carlo (MC) simulations, are tabulated in Appendix B.

4 RESULTS

The goal of the stellar population analysis is to gain insight into the SF and assembly history. Our approach is twofold. Here we analyse the radial properties as well as integrated (central) population parameters of our galaxies, in search of commonalities and/or differences within the sample. In the subsequent paper (Ryś et al., in preparation) we will take these results and, together with the results

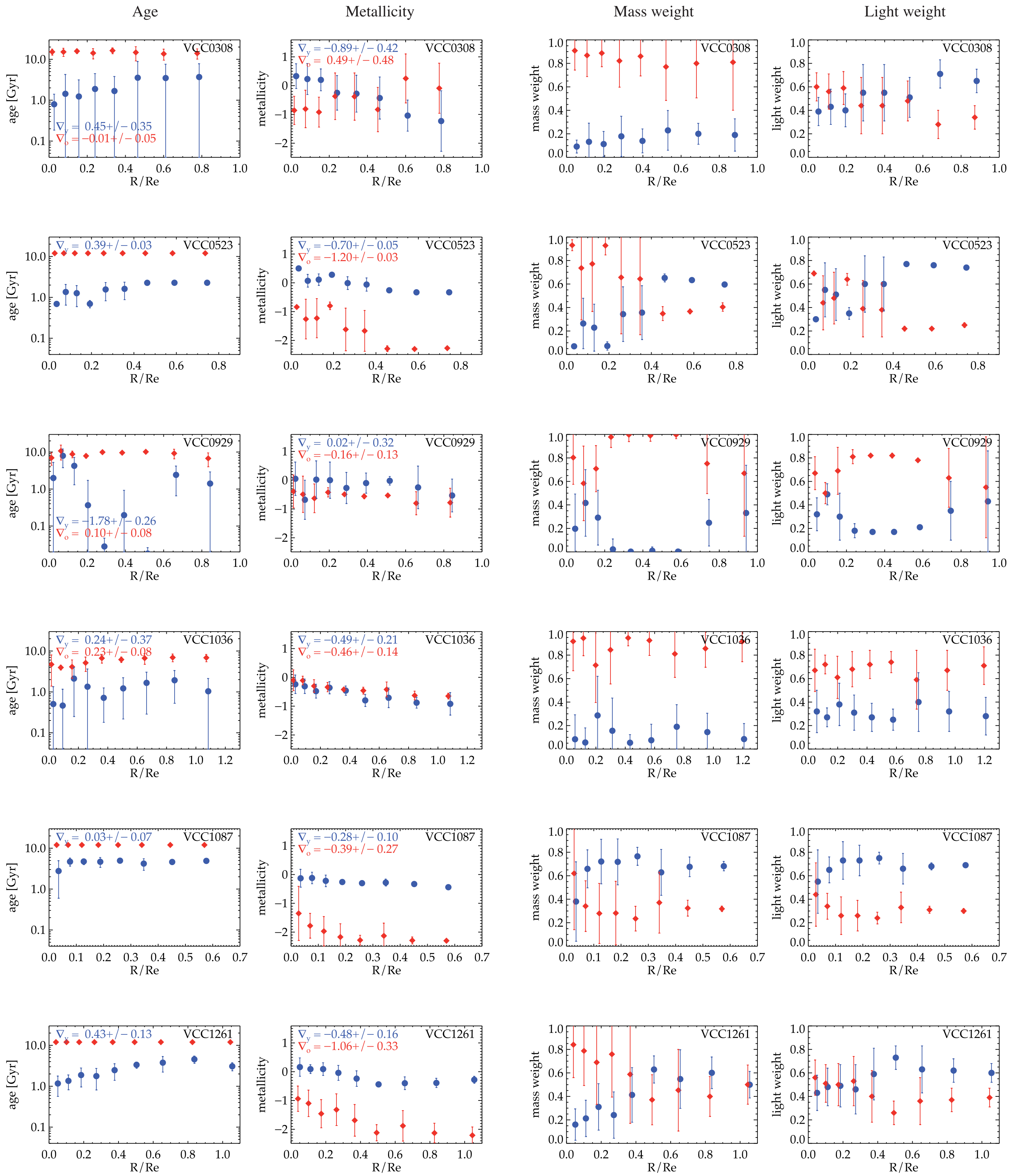

Figure 3. SFHs extracted from our 2D data collapsed in annuli of increasing width. Younger populations are shown with blue circles and the older ones with red diamonds (for NGC 3073 the intermediate population is shown with green triangles). The four columns show (respectively) age, metallicity (total metallicity in solar units), mass weight and light weight values, together with their errors, as a function of major axis effective radius. For VCC 0308, VCC 0929, VCC 1036, VCC 1431, NGC 3073 and ID 0918 we show fits for which no constraints were placed on the ages of the SSPs. For the remaining six galaxies the age of the older population was fixed to 12 Gyr. The given weight values are relative, i.e. at any given radius they add up to 1.0. A small horizontal offset was added to the old population so as to make the visual appearance of the points and their errors clearer.

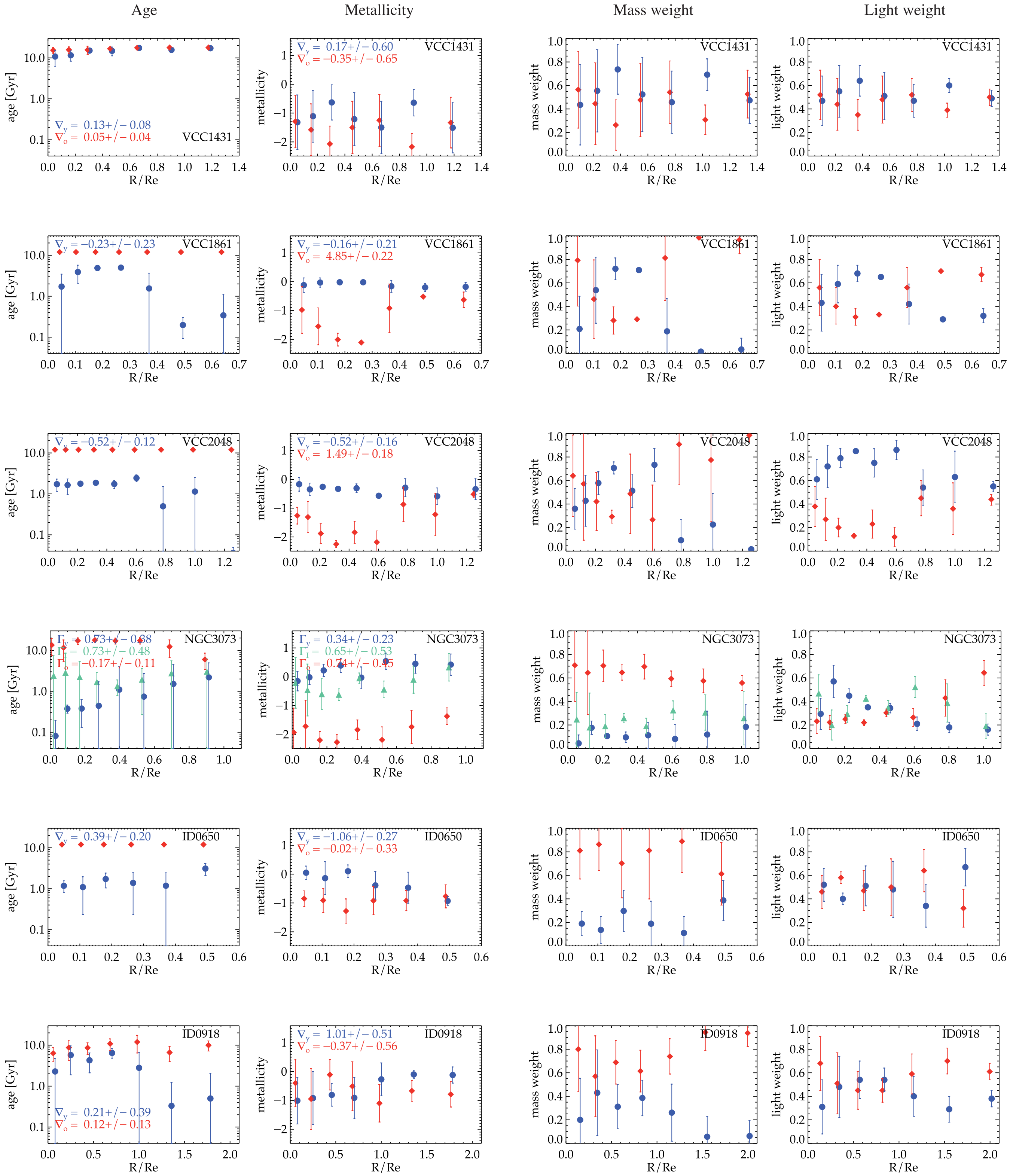

Figure 3 – *continued*

from LS analysis, will juxtapose them with those for more massive galaxies to look for potential (dis)similarities between the various galaxy classes.

4.1 SAURON versus SDSS star formation histories

SFHs were until recently extracted only in the cases where significantly longer wavelength (λ) ranges were available. This is generally required given the inherent degeneracies in stellar population parameters where ages and metallicities cannot be easily separated. One thus aims to include as broad a range of features (i.e. have a long λ coverage) as possible to minimize these effects. With SAURON the available wavelength range (4760–5300 Å) is rather limited; however, high S/N values can provide a leverage against the λ range in the context of SFH recovery. This was recently tested for giant early-type galaxies from the ATLAS3D sample by McDermid et al. (2015). Their results show that there is no systematic bias between the SDSS and SAURON extracted SFHs (see their section 2.6 for details.)

To see whether the results would hold also for our low-mass galaxies, we have extracted SFHs for the SDSS data, which provide central 3-arcsec spectroscopic information for a number of galaxies as a part of the survey. SDSS presented itself as our natural choice, given that its spectroscopic sample had 10 objects in common with ours and the available wavelength range is extended (3800–9200 Å[3]). At the same time SDSS data have significantly lower S/N given predominantly much shorter exposure times (between 2400 and 5400 s). The results of the analysis are shown in Fig. 2 and tabulated in Table 2. The three data sets were compared with one another and for the majority of objects the recovered ages, metallicities and mass weights (i.e. the relative amounts of stellar masses contained in old and young populations) agree to within the errors. Outlying values belong to different data sets for different galaxies, that is, there are no systematic trends present. We note, however, that for the second data set – SDSS with the SAURON λ range – the values tend to deviate from the other more often, suggesting that in this case low S/N *together with* limited λ range increases the uncertainties.

We can see that, in general, the recovery of metallicity for the younger component is quite good. This is expected as the age/metallicity degeneracy is more severe for old populations. The strongest outlier (middle left panel) is VCC 1431 for which we find nearly null fractions of the younger population, which is later confirmed in the full radial profiles analysis in the subsequent sections.

We conclude that agreement between the data sets is reasonably good, most of the existing discrepancies are caused by random errors and that our results presented in the subsequent sections are robust. Nevertheless, we note that the main focus of the exercise was to determine the suitability of the rather limited SAURON range, rather than an absolute comparison between the data sets.

4.2 Star formation histories

Fig. 3 shows 2-SSP SFHs for our sample, where the ages and metallicities of both young and old components are shown for each galaxy (Columns 1 and 2) together with the mass and light weights of both populations (Columns 3 and 4).

Among the galaxies for which we did not fix the age of the old population to 12 Gyr, for two of the objects we found non-negligible contributions from intermediate-aged components, with ages between [3,10] Gyr. For the remaining four (VCC 0308, VCC 1431, NGC 3073, and ID 0918) we found ages in the range of $\gtrsim$ 10–13 Gyr.

The old components of VCC 1431 and VCC 0308 have the maximum allowed ages. VCC 0308 is our only 'blue centre' galaxy in the sample, i.e. it is an object whose photometry indicates recent central SF episodes and indeed the age of the young population is as low as <1 Gyr in the centre. VCC 1431 is an interesting case since here the recovered age of the younger population practically coincides with that of the old one. No significant SF activity seems to have taken place there at least in the last 10 Gyr in the centre and 12–13 Gyr in the outskirts.

In eight objects the old population dominates the mass at all radii. Interestingly, in the case of two galaxies (VCC 0523 and VCC 1261) the relative contribution of younger population increases with radius. In another two (VCC 1861 and less strongly VCC 2048) we see a young population 'bump' at around 0.2–0.4 R_e, which subsequently goes to zero. The remaining weight profiles are flat to within the errors.

There are positive age gradients present in the younger populations of seven of our galaxies, with the remaining five showing the overall gradient values consistent with zero. In the case of VCC 0929, belonging to the latter group, there is an increase in the young population age at around 0.1 $R_{\rm e}$ and the profile flattens out for larger radii. The population's weights are, however, nearly zero, so we do not interpret the above feature as significant. A similar, though shallower, feature can be seen in the profile of VCC 1861. Noting that the young population weights drop to zero for larger radii we can conclude that the central 0.3 $R_{\rm e}$ shows a young population presence with a positive age gradient.

We see a slight age gradient in the older population of VCC 1036 (of an intermediate age in this case) and a compound age gradient in ID 0918, where a clear positive radial age trend is broken at ∼1.2 $R_{\rm e}$ for both populations, with the ages being much lower for larger radii but again seeming to pick up a positive trend there as well. All the other gradients are nearly or fully consistent with zero. We note that this is not an indication of the lack of gradients but rather a result of the inherent difficulties in model resolution at those higher ages.

Metallicities of young populations are higher than or equal to those of old populations, with the former on average around the solar value in the centres and declining outwards or remaining constant, and the latter approximately in the range (0, −2) and showing a similar outward trend.

One third of our objects show the presence of a metallicity gradient in their older populations. These are VCC 0523, VCC 1087 (where the ages themselves are fixed to 12 Gyr), VCC 1036 and VCC 1261 (where the ages are intermediate, i.e. up to 10 Gyr). For the remaining objects the gradients are nearly or fully consistent with zero.

Young populations show a larger spread in metallicity gradient values. Half of the sample shows negative gradients, four of which are strong, i.e. with $\nabla_Z > 0.5$ dex. Three objects have gradients consistent with zero and the remaining three have positive ones. To the last group belongs ID 0918 where the trend is actually composed of two flat profiles with a break at around 1.2 $R_{\rm e}$: the outer profile is higher by ∼0.8 dex. A similar but less pronounced trend is seen in VCC 2048, this time with the difference being around 0.4 dex and the break radius at ∼0.6 $R_{\rm e}$. Here also the weights of the younger component fall to nearly zero above the quoted radius. So it is more correct to interpret the profiles as having a young

[3] https://www.sdss3.org/dr9/spectro/spectro_basics.php

Table 2. Tabulated results of the comparison between the SFHs extracted from the SDSS and central SAURON data. For each galaxy the first row shows the results from the fitting of full SDSS wavelength range, the second – SDSS restricted to the wavelength range of SAURON, and the third – central 3 arcsec of our SAURON data. Note that for some galaxies the age of the old population was fixed to 12 Gyr, hence the 0.00 errors.

Object	Age (young) (Gyr)	Z (young) ($Z_\odot$)	Weight(young)	Age (old) (Gyr)	Z (old) ($Z_\odot$)	Weight (old)
ID0650	3.1 ± 0.4	0.3 ± 0.2	0.57	12.0 ± 0.0	-1.0 ± 0.3	0.43
	1.3 ± 0.7	0.3 ± 0.4	0.15	12.0 ± 0.0	-0.6 ± 0.3	0.85
	1.7 ± 0.1	0.3 ± 0.1	0.36	12.0 ± 0.0	-1.3 ± 0.1	0.64
ID0918	5.0 ± 0.0	0.0 ± 0.1	0.86	12.3 ± 4.1	-1.3 ± 0.2	0.14
	1.2 ± 0.4	0.4 ± 0.3	0.05	16.6 ± 2.9	-0.4 ± 0.0	0.95
	5.0 ± 0.0	-0.1 ± 0.0	0.94	5.0 ± 0.0	-2.3 ± 0.0	0.06
VCC 0523	1.0 ± 0.0	0.5 ± 0.0	0.21	12.0 ± 0.0	-0.8 ± 0.1	0.79
	1.9 ± 0.3	0.1 ± 0.0	1.00	12.0 ± 0.0	-0.4 ± 0.5	0.00
	0.8 ± 0.0	0.4 ± 0.0	0.08	12.0 ± 0.0	-0.8 ± 0.0	0.92
VCC 0929	5.0 ± 0.0	-0.1 ± 0.1	0.95	9.5 ± 8.6	-2.2 ± 0.7	0.05
	2.1 ± 0.3	0.7 ± 0.0	0.16	10.4 ± 2.5	-0.6 ± 0.1	0.84
	5.0 ± 0.0	0.6 ± 0.0	0.41	5.9 ± 0.4	-0.8 ± 0.0	0.59
VCC 1036	2.9 ± 0.3	0.3 ± 0.1	0.71	10.7 ± 4.7	-1.4 ± 0.3	0.29
	2.4 ± 0.3	0.1 ± 0.1	0.94	18.0 ± 14.7	-2.3 ± 2.9	0.06
	2.9 ± 0.1	0.1 ± 0.0	0.61	17.2 ± 1.0	-1.7 ± 0.1	0.39
VCC 1087	4.9 ± 5.1	0.7 ± 0.5	0.16	5.8 ± 1.4	-0.4 ± 0.2	0.84
	4.8 ± 1.7	0.1 ± 0.2	0.83	8.3 ± 4.2	-2.3 ± 0.0	0.17
	0.1 ± 0.0	0.0 ± 0.3	0.01	6.8 ± 0.6	-0.4 ± 0.0	0.99
VCC 1261	1.7 ± 0.4	0.3 ± 0.1	0.32	12.0 ± 0.0	-1.1 ± 0.2	0.68
	2.4 ± 0.3	0.0 ± 0.2	0.74	12.0 ± 0.0	-1.9 ± 0.9	0.26
	0.9 ± 0.1	0.4 ± 0.1	0.09	12.0 ± 0.0	-0.8 ± 0.0	0.91
VCC 1431	5.0 ± 1.8	-1.0 ± 0.0	0.14	10.4 ± 2.4	-0.4 ± 0.0	0.86
	0.3 ± 0.7	-0.3 ± 2.5	0.00	13.8 ± 7.4	-0.6 ± 0.1	1.00
	0.1 ± 0.0	-0.1 ± 0.1	0.00	12.8 ± 1.0	-0.6 ± 0.0	1.00
VCC 1861	1.3 ± 0.6	0.5 ± 0.3	0.08	7.2 ± 2.6	-0.4 ± 0.1	0.92
	3.6 ± 3.9	0.7 ± 0.0	0.46	5.0 ± 0.0	-0.7 ± 0.4	0.54
	5.0 ± 0.0	-0.1 ± 0.1	0.81	6.1 ± 0.7	-1.8 ± 0.2	0.19
VCC 2048	4.3 ± 0.6	-0.1 ± 0.1	0.70	12.0 ± 0.0	-1.7 ± 0.1	0.30
	2.7 ± 0.4	0.1 ± 0.2	0.65	12.0 ± 0.0	-1.7 ± 0.7	0.35
	1.1 ± 0.0	0.1 ± 0.0	0.11	12.0 ± 0.0	-1.0 ± 0.0	0.89

component that is restricted to the inner 0.5 R_e. NGC 3073's positive metallicity trend may be related to the galaxy being in the vicinity and under the tidal influence of the larger NGC 3079, but this would require some mixing of stellar material coming from the large neighbour.

5 DISCUSSION AND CONCLUSIONS

5.1 Star formation histories

First attempts at providing SFHs of Virgo dEs are in Lisker et al. (2006b) where they used the 3-arcsec SDSS spectra for a sample of 16 dEs, nine of which were classified as hosting a blue core. Not meant to be a fully-fledged SFH analysis, the results provided rough estimates on the age ranges of the studied objects. The study showed that all their galaxies had an underlying old population (with the age fixed at 5 Gyr) in their centres, accounting for at least 90 per cent of the total mass, albeit contributing only a small fraction to the total galaxy light there. Koleva et al. (2009a) were the first to attempt a full SFH reconstruction, also spatially resolving their data into two bins (central and 1 R_e apertures). These authors confirmed the presence of old ($\gtrsim$10 Gyr) populations in all but one of their galaxies. Interestingly, for about half of their sample they find constant/slowly declining SFHs, indicative of fairly continuous SF activity from the early ages until recently. They concluded that the galaxies could not have been stripped of their gas early on in their evolution and that the ages of old populations are comparable with those of massive ETGs, with the difference being that dE SF efficiency is lower. This also holds true for lower mass systems in the LG where all studied dwarf types have shown evidence for the presence of older ages (see the review of Tolstoy et al. 2009 and references therein).

Our results agree with those previous findings. We, too, find old or intermediate populations in all our objects, even more so, one of our galaxies seems to contain *only* an old population with the age over $\gtrsim$10 Gyr (see the following subsection). Interestingly, very similar results are found by Hidalgo et al. (2013) in their SFH results for four LG dwarfs (spheroidal and transitional type): the oldest populations are coeval across all probed radii, with the young components more prominent and younger in the inner regions (see their figs 9 and 10). The mass difference between their and our sample is, naturally, significant, yet, the profile similarities are remarkable.

Seeing extended SFHs and/or multiple SF episodes in the majority of our objects further strengthens the conclusion of Paper II where we show that dEs have higher concentration and steeper rotation curves than their presumed late-type progenitors. We said there that either it could be due to harassment or it could also mean that the real progenitors were also more compact [e.g. blue compact dwarf (BCD) like objects]. This has been suggested earlier by e.g. Koleva et al. (2009b) who proposed BCDs as the progenitors of dEs with steep metallicity gradients. We have added a dynamical/kinematic weight to the argument (note, however, that we find gradients in one third of our sample and the rest of our galaxies show null gradient values). While we are not in the position yet to decisively confirm or reject either hypothesis, at least the former scenario seems compatible with our latest results presented in this work.

The discovery of those oldest stellar populations underlying four galaxies in our sample and the majority of dEs studied so far provides support to the claim that they contributed to the build-up of the outskirts of massive galaxies. So far we have claimed otherwise (e.g. in Ryś & Falcón-Barroso 2012) since massive ETGs showed older ages based on SSP estimates. The SSP ages of both types are, however, biased by the light coming from young(er) populations, if they are present. We now know this to be the case for dEs. We can thus envision a scenario in which *some* of the dE *progenitors* were the material used in the build-up of the haloes of more massive galaxies, with the remaining gas being transformed into stars early on. Those that survived would then go through the transformation steps proposed here earlier (and elsewhere in the literature), namely undergoing later episodes of SF induced by (among others) the tidal forces of the cluster. Naturally, detailed chemical analyses will be needed to confirm this statement; in particular we should look at chemical abundances in massive ellipticals out to several effective radii, which should ideally be complemented with these properties' redshift dependence.

5.2 A genuinely old system?

The analysis of one of our galaxies, VCC 1431, reveals no evidence for stellar populations younger than ∼10 Gyr, i.e. what we see in its SFH is a uniformly old population across the entire analysed area, in this case 1.5 effective radii. The galaxy, a nucleated dE, does not show evidence for any type of substructure such as a disc or spiral arms (Janz et al. 2014). Thus there are no tell-tale sign of interaction present. Could this object be genuinely old?

On the one hand, following the prevailing ideas on how dE galaxies came to be, we should assume the infall scenario. The galaxy's projected distance from the Virgo's central galaxy M87 is only $1\overset{\circ}{.}19$ and thanks to the surface brightness fluctuation-based line-of sight distance (Mei et al. 2007) we know that its true, intrinsic location is also a central one. Our previous results on the dynamical properties of the galaxy (see Paper II) show it to have one of the lowest angular momentum values and steepest circular velocity profile of our cluster dwarfs. We therefore conclude that the object had its SF quenched through ram-pressure stripping before it entered the cluster environment (e.g. in a group setting[4] and subsequent tidal influence lowered its angular momentum and heated the galaxy, making it more compact and rounder ($\epsilon = 0.03$), in agreement with Moore et al. (1998).

On the other hand, only because a galaxy is situated close to the cluster centre does not necessarily mean that something must have happened to it that left obvious traces. It may be sufficiently compact in radius that its tidal radius is well outside the baryonic one (see Penny et al. 2009). And it may happen to be on an orbit with little eccentricity, in which case there would be little variation of the tidal forces and thus also no need to trigger a SF burst. Again, in ΛCDM one would expect to have a number of galaxies that have never 'fallen in' but have instead 'been there' (i.e. alongside the most massive progenitor) since the beginning. This seems to be another plausible evolution scenario for VCC 1431.

In either case, the finding needs to be understood and explained in the context of what we know about the formation and evolution of dE galaxies. Is VCC 1431 a relic that has evolved *in situ* and has survived intact over (at least) the last few Gyr because of its compactness, or was the galaxy's SF indeed quenched long ago, before it entered the cluster environment, but tidal interactions heated the body of the galaxy, altering its mass profile and/or rotational properties? One way to address these questions would be to try and find objects of similar mass and structure in cosmological simulations and trace their evolution back to before they became satellites [see Stringer et al. (2015) for such an analysis of compact giant ellipticals based on the Trujillo et al. (2014) results for NGC 1277]. This could provide more insight on the possible evolutionary paths of such objects.

5.3 The puzzle of an isolated galaxy

For the field galaxy ID 0918 we see a correlation between the stellar populations radial trends and its kinematic properties. Both young and old populations have a break in their profile at around 1.2 R_e, which radius corresponds to the size of the KDC reported in Ryś et al. (2013). The clear positive radial age trend is broken at the KDC radius for both populations, with the ages being much lower for larger radii but again seeming to pick up a positive trend there as well. The younger population's metallicity profile is flat both inside and outside of the KDC region but the latter values are on average higher by 0.8 dex.

This is an unusual trend which could be explained if we assume that the KDC is a result of a merger of two dwarf galaxies, with the material from the smaller accreted dwarf being the explanation for the younger ages and higher metallicities in the outskirts of ID 0918. Because the trends are not smoothed out we could conclude that when the merger happened, both galaxies must have already lost their gas reservoirs and no further SF took place. For this explanation to be correct, the merger must have happened within the last ∼1 Gyr. Unfortunately, no deep imaging – where, e.g. tidal tails could be spotted – of the region is currently available to confirm or disprove the theory. On the other hand, the lower metallicity of the younger population in the central parts could be explained if some stellar population/material mixing has taken place.

No similar trend, i.e. no stellar population signature, is seen for the other field dwarf hosting a KDC, i.e. ID 0650. A possible explanation for the difference could be the time at which each presumed merger occurred: long enough ago for the stellar population differences to have been diluted in ID 0650. The availability of gas might also have induced a SF episode which smoothed the differences between the two components.

The relative isolation of the galaxies – no similarly sized or larger objects within a projected radius of 20 arcmin – makes the suggested merger in principle a highly unlikely event. ID 0918 must, therefore, be a result of a particular coincidence of progenitor galaxies' initial orbits which led to the suggested merger. No other theory currently exists that would be able to explain the above findings. It would, naturally, be interesting to investigate similar environments and galaxies residing in them in search of (dis)similarities with ID 0918,

[4] A number of recent works, both observational and theoretical, suggest that ram-pressure stripping is more efficient than we used to think (see the discussion in Kormendy & Bender 2012 and the references therein); also, a good illustration of ram-pressure stripping at work in a group environment is the morphology–density relation of the Milky Way/M31 groups of satellite galaxies (Mateo 2008).

and also to carry out simulations which could shed some light on its exact formation path.

6 SUMMARY AND FUTURE WORK

We have presented the stellar population analysis of a sample of 12 DEs coming from our SAURON study of Virgo and field dE objects. We have shown that with high quality unresolved spectroscopic data we are able to recover SFHs in the sense of decomposing our galaxies into two stellar populations. Additionally, by employing 3D data and using values averaged along annuli the derived properties are not biased towards a specific axis and as such are more robust than long-slit data.

We find that the majority of our dEs either still exhibited significant SF a few Gyr ago or experienced a secondary burst of SF that occurred roughly at that time. We interpret this as a tentative piece of evidence in favour of a harassment scenario, where such episodes of SF are expected as the remaining gas is driven inwards as a result of tidal forces.

We also find that the old populations of some of our dEs are roughly coeval with those of giant ETGs, in principle making it possible for the *progenitors* of those dEs to have contributed to the build-up of the outskirts of massive galaxies – the younger SSP ages of dEs simply reflecting a more extended SF in later epochs. A detailed comparison of stellar population properties of dwarf and giant early-type galaxies based on LS analysis is the focus of our subsequent paper (Ryś et al., in preparation).

We find a correlation between the stellar population and kinematic properties of the field galaxy ID 0918. The metallicity and age profiles show a break at a radius which corresponds to the size of the KDC we earlier found in this galaxy (Ryś et al. 2013). We believe it to be an argument in favour of a merger origin of the KDC.

Finally, one of our galaxies, VCC 1431, does not show any sign of younger populations across the probed spatial extent (∼1.5 effective radii). We conclude that it either was ram-pressure stripped early on in its evolution in a group environment and subsequently tidally heated (which lowered its angular momentum and increased compactness), or that it evolved *in situ* in the cluster's central parts, compact enough to avoid tidal disruption.

Challenges related to observing the progenitor class of dEs are numerous. While it is intrinsically hard to accurately assess structural parameters of high-redshift galaxies to compare them with what we see in the nearby Universe, in the case of dEs we do not even have the luxury of having candidate progenitors at higher z. The reason is not the uncertain evolution path which makes the progenitor search complex – after all if a given galaxy is a relic we are simply looking for an object with characteristics matching that galaxy as closely as possible. The problem is the low masses / luminosities of dEs which virtually preclude high-z observations of objects with similar structural characteristics.

We can hope that once large samples for environments of varying density have been analysed, more answers will emerge. It would also be of vital importance to be able to test our observational results against a larger suite of simulations. So far in works dedicated to studying the influence of tidal forces on cluster dwarfs we have dealt with remnants which were more massive (Moore et al. 1998) or more compact than our typical dwarfs (Smith, Davies & Nelson 2010) or have explored a limited set of initial structural parameters (Mastropietro et al. 2005). Ideally, one would also want to compare observations and simulations from as close a perspective as possible, by creating mock data sets (see e.g. Naab et al. 2014) and applying those same tools to their analysis as one does to real data. In this way our interpretation of the latter could be more robust.

ACKNOWLEDGEMENTS

AR is a postdoctoral fellow of the Alexander von Humboldt Foundation (Germany). MK is a fellow of the Fund for Scientific Research Flanders, Belgium (FWO). JFB acknowledges support from grant AYA2013-48226-C3-1-P from the Spanish Ministry of Economy and Competitiveness (MINECO). The paper is based on observations obtained at the William Herschel Telescope, operated by the Isaac Newton Group in the Spanish Observatorio del Roque de los Muchachos of the Instituto de Astrofísica de Canarias. We thank the referee, Richard McDermid, for his constructive comments and suggestions, which have helped optimize the presentation of this work. AR thanks Harald Kuntschner for comments on the draft version of this paper.

Funding for the SDSS and SDSS-II has been provided by the Alfred P. Sloan Foundation, the Participating Institutions, the National Science Foundation, the U.S. Department of Energy, the National Aeronautics and Space Administration, the Japanese Monbukagakusho, the Max Planck Society, and the Higher Education Funding Council for England. The SDSS Web site is http://www.sdss.org/.

REFERENCES

Baade W., 1944, ApJ, 100, 147
Bacon R. et al., 2001, MNRAS, 326, 23
Bender R., Burstein D., Faber S. M., 1992, ApJ, 399, 462
Binggeli B., 1994, in Hensler G., Theis C., Gallagher J. S., eds, Panchromatic View of Galaxies. Their Evolutionary Puzzle Dwarf Galaxies: A Morphological Overview. Editions Frontiers, Gif-sur-Yvette, p. 173
Binggeli B., Cameron L. M., 1991, A&A, 252, 27
Binggeli B., Sandage A., Tammann G. A., 1988, ARA&A, 26, 509
Cardiel N., Gorgas J., Sánchez-Blázquez P., Cenarro A. J., Pedraz S., Bruzual G., Klement J., 2003, A&A, 409, 511
Chung A., van Gorkom J. H., Kenney J. D. P., Vollmer B., 2007, ApJ, 659, L115
De Rijcke S., Dejonghe H., Zeilinger W. W., Hau G. K. T., 2004, A&A, 426, 53
Falcón-Barroso J., Sánchez-Blázquez P., Vazdekis A., Ricciardelli E., Cardiel N., Cenarro A. J., Gorgas J., Peletier R. F., 2011, A&A, 532, A95
Geha M., Guhathakurta P., van der Marel R. P., 2005, AJ, 129, 2617
Geha M., van der Marel R. P., Guhathakurta P., Gilbert K. M., Kalirai J., Kirby E. N., 2010, ApJ, 711, 361
Guerou A. et al., 2015, ApJ, 804, 70
Gunn J. E., Gott J. R., III, 1972, ApJ, 176, 1
Hidalgo S. L. et al., 2013, ApJ, 778, 103
Janz J. et al., 2012, ApJ, 745, L24
Janz J. et al., 2014, ApJ, 786, 105
Jerjen H., Kalnajs A., Binggeli B., 2000, A&A, 358, 845
Koleva M., de Rijcke S., Prugniel P., Zeilinger W. W., Michielsen D., 2009a, MNRAS, 396, 2133
Koleva M., Prugniel P., Bouchard A., Wu Y., 2009b, A&A, 501, 1269
Koleva M., Prugniel P., de Rijcke S., Zeilinger W. W., 2011, MNRAS, 417, 1643
Kormendy J., 1985, ApJ, 295, 73
Kormendy J., Bender R., 2012, ApJS, 198, 2
Le Borgne D., Rocca-Volmerange B., Prugniel P., Lançon A., Fioc M., Soubiran C., 2004, A&A, 425, 881
Lin D. N. C., Faber S. M., 1983, ApJ, 266, L21
Lisker T., Grebel E. K., Binggeli B., 2006a, AJ, 132, 497

Lisker T., Glatt K., Westera P., Grebel E. K., 2006b, AJ, 132, 2432
Lisker T., Grebel E. K., Binggeli B., Glatt K., 2007, ApJ, 660, 1186
Lisker T., Weinmann S. M., Janz J., Meyer H. T., 2013, MNRAS, 432, 1162
McDermid R. M. et al., 2015, MNRAS, 448, 3484
Mastropietro C., Moore B., Mayer L., Debattista V. P., Piffaretti R., Stadel J., 2005, MNRAS, 364, 607
Mateo M., 2008, The Messenger, 134, 3
Mei S. et al., 2007, ApJ, 655, 144
Moore B., Lake G., Katz N., 1998, ApJ, 495, 139
Naab T. et al., 2014, MNRAS, 444, 3357
Penny S. J., Conselice C. J., De Rijcke S., Held E. V., 2009, Astron. Nachr., 330, 991
Prugniel P., Soubiran C., 2001, A&A, 369, 1048
Ryś A., Falcón-Barroso J., 2012, Dwarf Galaxies: Keys to Galaxy Formation and Evolution. Springer-Verlag, Berlin - Heidelberg, p. 155
Ryś A., Falcón-Barroso J., van de Ven G., 2013, MNRAS, 428, 2980
Ryś A., van de Ven G., Falcón-Barroso J., 2014, MNRAS, 439, 284 (Paper II)
Skillman E. D., Bender R., 1995, in Pena M., Kurtz S., eds, Rev. Mex. Astron. Astrofis. Conf. Ser. Vol. 3. The Dwarf Galaxy Star Formation Crisis (Invited paper). Revista Mexicana de Astronomia y Astrofisica, p. 25
Smith R., Davies J. I., Nelson A. H., 2010, MNRAS, 405, 1723
Stringer M., Trujillo I., Dalla Vecchia C., Martinez-Valpuesta I., 2015, MNRAS, 449, 2396
Toloba E., Boselli A., Peletier R. F., Falcón-Barroso J., van de Ven G., Gorgas J., 2012, A&A, 548, A78
Toloba E. et al., 2014, ApJ, 783, 120
Tolstoy E., Hill V., Tosi M., 2009, ARA&A, 47, 371
Trujillo I., Ferré-Mateu A., Balcells M., Vazdekis A., Sánchez-Blázquez P., 2014, ApJ, 780, L20
Vazdekis A., Sánchez-Blázquez P., Falcón-Barroso J., Cenarro A. J., Beasley M. A., Cardiel N., Gorgas J., Peletier R. F., 2010, MNRAS, 404, 1639
Vazdekis A., Ricciardelli E., Cenarro A. J., Rivero-González J. G., Díaz-García L. A., Falcón-Barroso J., 2012, MNRAS, 424, 157

APPENDIX A: COMPARISON OF 2-SSP ULYSS SFHS WITH LINE-STRENGTH-BASED STELLAR POPULATION VALUES

While a detailed analysis of LS and LS-based stellar population parameters will be the subject of our forthcoming paper, we present here a comparison between them and the SFHs presented in this work. The LS values shown in Fig. A1 have been used to obtain ages and metallicities and their errors with the use of the RMODEL software of Cardiel et al. (2003). For a detailed description we refer the reader to the above paper. In short, the program, using as input LS indices, determines ages and metallicities through the interpolation in SSP model predictions, in this case MILES models of Falcón-Barroso et al. (2011). Both linear and bivariate fits are computed to perform the interpolation, with the latter adopted for our purposes. The errors on the parameters are estimated by running MC simulations, making use of the uncertainties introduced for each LS index.

This comparison is intended as a consistency check between the two independent methods, also given the complex nature of multiple-SSP approach applied to unresolved data. Fig. A2 shows that for most of the galaxies we find a good agreement between the SFH luminosity-weighted and LS-based ages and metallicities, particularly in the innermost (typically younger) regions. Below we comment on those objects for which some systematic deviations are found, noting, however, that most of them still agree to within the errors. Our overall conclusion is that nearly consistent results are obtained for most galaxies.

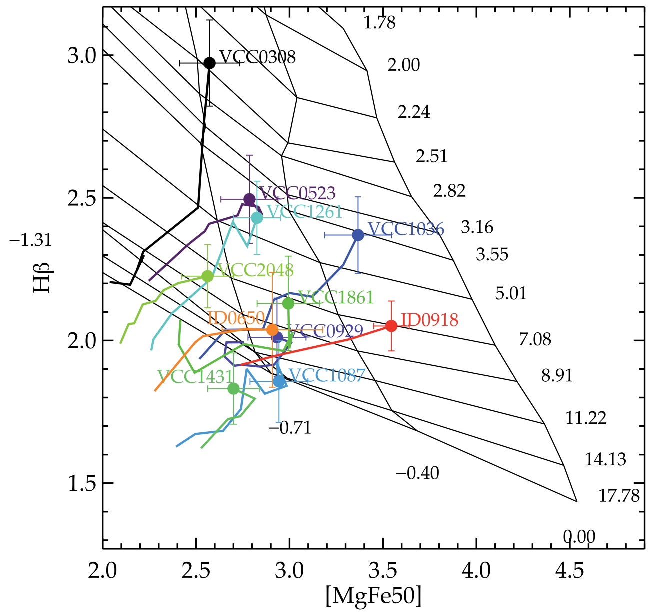

Figure A1. Left: Hβ versus [MgFe50] LS gradients averaged along isophotes, overplotted on MILES model predictions of Falcón-Barroso et al. (2011). Galaxy centres are marked with filled dots and their error bars are also provided. The values are shown up to 1 effective radius, unless the radial extent of the data is smaller. NGC 3073 is not shown as it falls off the *y*-axis at younger ages – the plotting range has been adjusted to emphasize the differences among the cluster galaxies.

For VCC0 308 the LS results suggest lower metallicity, which does not translate into an older population in the inner region (i.e. against the age/metallicity degeneracy expectations). In the case of VCC 0929 there is a systematic difference in age, which is compensated by a difference in metallicity. For VCC 1087 the agreement is good given the quite old ages; however, some disagreement is seen in the very centre, and the age/metallicity degeneracy might be at work. VCC 1261 innermost regions show lower LS metallicities, while ages are in good agreement. In the case of ID 0918 the SFH metallicities in the centre are lower than the LS-based values, with an opposite trend in the outer parts.

APPENDIX B: ULYSS-EXTRACTED POPULATION PARAMETERS

MC simulations are performed to estimate errors, and the coupling (i.e. degeneracies) between the parameters. Table B1 shows the ULySS-extracted SFHs including MC simulation results for all radial bins and galaxies. The simulations consist of series of analyses of a spectrum with added random noise corresponding to the noise estimated from the data (200 realizations in each case), computed to produce χ^2 close to 1. The added noise has a Gaussian distribution and takes into account the correlation between the pixels introduced along the processing. This effect is modelled by keeping track of the number of independent pixels during the steps of the processing, and then generating a random vector of independent points which is eventually resampled to the actual length of the spectrum (see section 2 and 3.3 of Koleva et al. 2009b for more details).

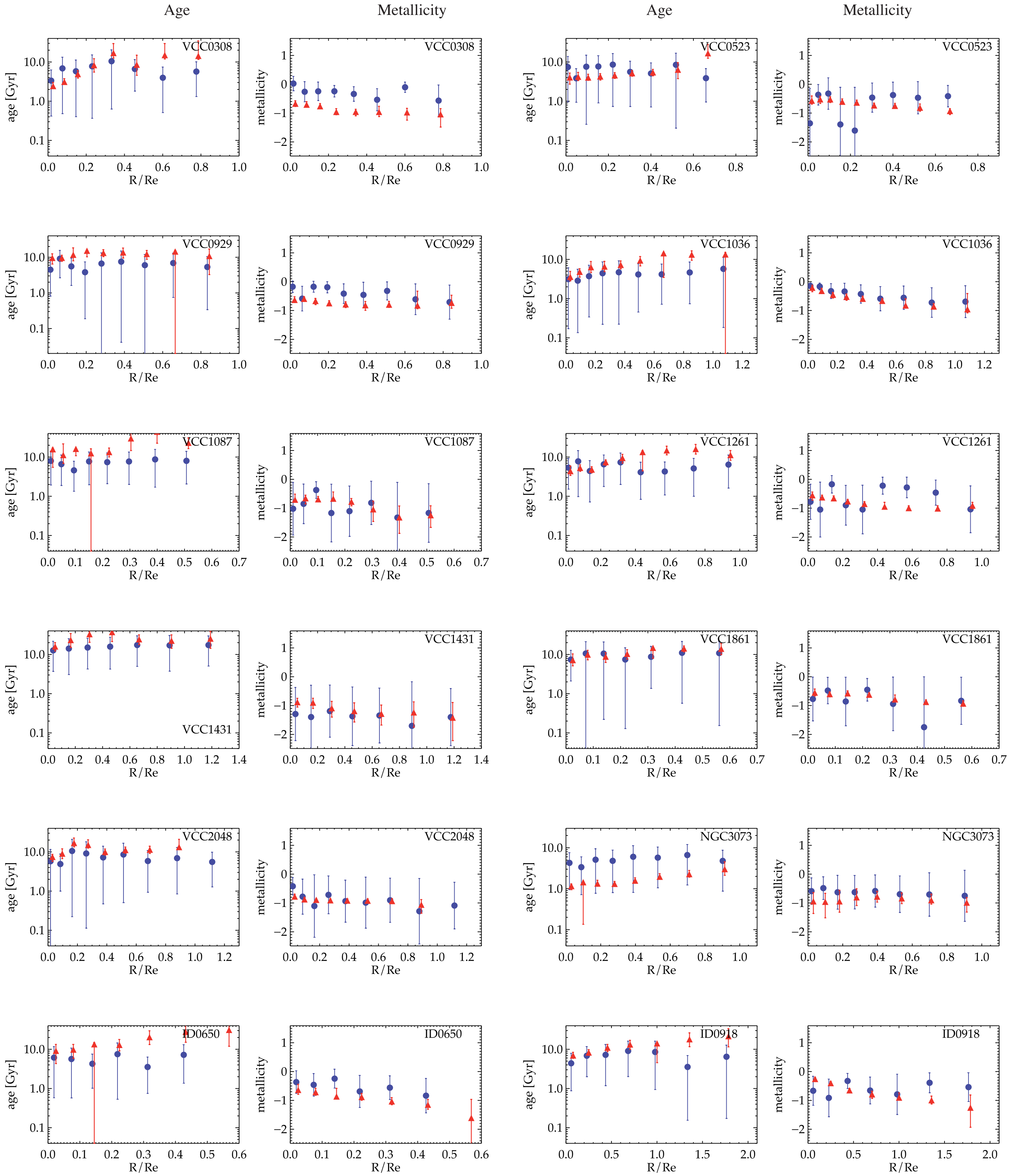

Figure A2. Comparison of luminosity weighted profiles from the SFHs presented in this work (blue filled circles) with the profiles of SSP age and *Z* values from our LS analysis (red filled triangles) to be presented in Ryś et al. (in preparation). Error estimates for the LS-based values are shown for the innermost bins.

Table B1. Results of the ULySS MC simulations.

r (arcsec)	Age (young) (Myr)	Z (young) ($Z_{\odot}$)	Age (old) Myr	Z (old) ($Z_{\odot}$)
		VCC 0308		
1.00000	795 ± 610	+0.33 ± 0.43	15215 ± 2530	−0.86 ± 0.49
2.20000	1433 ± 2826	+0.23 ± 0.54	15173 ± 3413	−0.81 ± 0.65
3.64000	1233 ± 1907	+0.20 ± 0.38	15849 ± 1981	−0.92 ± 0.52
5.37000	1881 ± 2593	−0.25 ± 0.60	14213 ± 3962	−0.37 ± 0.81
7.44000	1676 ± 2124	−0.28 ± 0.64	16365 ± 2638	−0.38 ± 0.82
9.93000	3543 ± 5323	−0.43 ± 0.73	14730 ± 5597	−0.83 ± 0.77
12.9100	3484 ± 4116	−1.04 ± 0.54	13635 ± 4080	+0.25 ± 0.85
16.4900	3690 ± 4107	−1.23 ± 1.05	14052 ± 3940	−0.09 ± 0.87
		VCC 0523		
1.00000	690 ± 74	+0.50 ± 0.07	11999 ± 0	−0.84 ± 0.03
2.20000	1354 ± 708	+0.07 ± 0.22	11999 ± 0	−1.26 ± 0.69
3.64000	1265 ± 672	+0.11 ± 0.20	11999 ± 0	−1.23 ± 0.68
5.37000	694 ± 140	+0.28 ± 0.07	11999 ± 0	−0.80 ± 0.13
7.44000	1561 ± 740	−0.01 ± 0.22	11999 ± 0	−1.62 ± 0.74
9.93000	1615 ± 738	−0.06 ± 0.23	11999 ± 0	−1.67 ± 0.71
12.9100	2268 ± 87	−0.26 ± 0.02	11999 ± 0	−2.29 ± 0.10
16.4900	2276 ± 26	−0.33 ± 0.02	11999 ± 0	−2.30 ± 0.01
20.7900	2276 ± 65	−0.33 ± 0.03	11999 ± 0	−2.27 ± 0.05
		VCC 0929		
1.00000	1985 ± 3246	+0.05 ± 0.58	6959 ± 2570	−0.39 ± 0.57
2.20000	7919 ± 4134	−0.68 ± 0.68	10731 ± 4661	−0.49 ± 0.63
3.64000	4237 ± 2935	+0.02 ± 0.65	8769 ± 1786	−0.63 ± 0.50
5.37000	365 ± 1345	−0.00 ± 0.63	7850 ± 1033	−0.42 ± 0.16
7.44000	28 ± 19	−0.27 ± 0.54	9921 ± 871	−0.49 ± 0.03
9.93000	197 ± 727	−0.10 ± 0.35	9588 ± 591	−0.56 ± 0.08
12.9100	18 ± 8	−0.02 ± 0.15	10151 ± 617	−0.53 ± 0.02
16.4900	2412 ± 1756	−0.25 ± 0.74	9212 ± 2659	−0.80 ± 0.40
20.7900	1406 ± 1499	−0.53 ± 0.57	6729 ± 2738	−0.78 ± 0.50
		VCC 1036		
1.00000	505 ± 840	−0.24 ± 0.32	4705 ± 3322	−0.10 ± 0.36
2.20000	463 ± 699	−0.31 ± 0.25	3956 ± 532	−0.11 ± 0.15
3.64000	2116 ± 1866	−0.48 ± 0.24	4110 ± 1956	−0.30 ± 0.22
5.37000	1341 ± 2294	−0.36 ± 0.21	5138 ± 1960	−0.34 ± 0.16
7.44000	716 ± 536	−0.46 ± 0.16	6677 ± 1612	−0.42 ± 0.04
9.93000	1219 ± 1002	−0.80 ± 0.21	6184 ± 964	−0.46 ± 0.12
12.9100	1665 ± 1378	−0.71 ± 0.34	6696 ± 1952	−0.42 ± 0.26
16.4900	1927 ± 1401	−0.88 ± 0.19	6944 ± 1490	−0.63 ± 0.15
20.7900	1037 ± 1092	−0.92 ± 0.39	6852 ± 1380	−0.65 ± 0.10
		VCC 1087		
1.00000	2767 ± 2170	−0.13 ± 0.31	11999 ± 0	−1.35 ± 0.94
2.20000	4688 ± 1033	−0.12 ± 0.20	11999 ± 0	−1.78 ± 0.43
3.64000	4731 ± 753	−0.22 ± 0.20	11999 ± 0	−1.97 ± 0.51
5.37000	4654 ± 1261	−0.26 ± 0.08	11999 ± 0	−2.17 ± 0.46
7.44000	4951 ± 479	−0.30 ± 0.02	11999 ± 0	−2.28 ± 0.17
9.93000	4201 ± 1321	−0.28 ± 0.12	11999 ± 0	−2.13 ± 0.44
12.9100	4604 ± 658	−0.33 ± 0.03	11999 ± 0	−2.29 ± 0.12
16.4900	4896 ± 340	−0.44 ± 0.04	11999 ± 0	−2.30 ± 0.01
		VCC 1261		
1.00000	1168 ± 605	+0.16 ± 0.32	11999 ± 0	−0.94 ± 0.44
2.20000	1354 ± 535	+0.09 ± 0.15	11999 ± 0	−1.10 ± 0.46
3.64000	1876 ± 914	+0.09 ± 0.22	11999 ± 0	−1.46 ± 0.49
5.37000	1770 ± 958	−0.04 ± 0.26	11999 ± 0	−1.32 ± 0.55
7.44000	2473 ± 1080	−0.24 ± 0.27	11999 ± 0	−1.69 ± 0.55
9.93000	3340 ± 578	−0.44 ± 0.09	11999 ± 0	−2.12 ± 0.28
12.9100	3775 ± 1553	−0.40 ± 0.22	11999 ± 0	−1.88 ± 0.53
16.4900	4566 ± 921	−0.39 ± 0.16	11999 ± 0	−2.13 ± 0.34
20.7900	3075 ± 688	−0.28 ± 0.12	11999 ± 0	−2.21 ± 0.29

Table B1 – *continued*

r (arcsec)	Age (young) (Myr)	*Z* (young) ($Z_\odot$)	Age (old) Myr	*Z* (old) ($Z_\odot$)
		VCC 1431		
1.00000	10797 ± 4528	−1.32 ± 0.95	15412 ± 2680	−1.29 ± 0.90
2.20000	11595 ± 3276	−1.11 ± 0.90	15812 ± 2857	−1.58 ± 0.90
3.64000	15073 ± 1616	−0.63 ± 0.61	15729 ± 3549	−2.07 ± 0.62
5.37000	14835 ± 3608	−1.21 ± 0.92	16758 ± 1672	−1.50 ± 0.91
7.44000	17477 ± 1853	−1.50 ± 0.91	17648 ± 619	−1.25 ± 0.90
9.93000	15722 ± 1716	−0.64 ± 0.46	17895 ± 439	−2.17 ± 0.46
12.9100	17202 ± 1861	−1.51 ± 0.87	17876 ± 378	−1.33 ± 0.88
		VCC 1861		
1.00000	1721 ± 1739	−0.12 ± 0.25	11999 ± 0	−0.98 ± 0.81
2.20000	3910 ± 1830	−0.03 ± 0.16	11999 ± 0	−1.55 ± 0.64
3.64000	4893 ± 579	−0.02 ± 0.09	11999 ± 0	−2.01 ± 0.22
5.37000	4999 ± 0	−0.02 ± 0.03	11999 ± 0	−2.11 ± 0.06
7.44000	1549 ± 2122	−0.16 ± 0.21	11999 ± 0	−0.92 ± 0.84
9.93000	198 ± 106	−0.20 ± 0.14	11999 ± 0	−0.52 ± 0.03
12.9100	342 ± 787	−0.18 ± 0.15	11999 ± 0	−0.63 ± 0.27
		VCC 2048		
1.00000	1727 ± 566	−0.17 ± 0.24	11999 ± 0	−1.26 ± 0.29
2.20000	1642 ± 680	−0.35 ± 0.22	11999 ± 0	−1.31 ± 0.54
3.64000	1773 ± 231	−0.26 ± 0.09	11999 ± 0	−1.88 ± 0.34
5.37000	1869 ± 107	−0.33 ± 0.04	11999 ± 0	−2.25 ± 0.12
7.44000	1741 ± 401	−0.31 ± 0.15	11999 ± 0	−1.84 ± 0.38
9.93000	2439 ± 464	−0.57 ± 0.05	11999 ± 0	−2.18 ± 0.39
12.9100	497 ± 1020	−0.29 ± 0.31	11999 ± 0	−0.87 ± 0.60
16.4900	1141 ± 1380	−0.59 ± 0.29	11999 ± 0	−1.22 ± 0.74
20.7900	36 ± 13	−0.34 ± 0.36	11999 ± 0	−0.52 ± 0.10
		ID0650		
1.00000	1179 ± 379	+0.05 ± 0.23	11999 ± 0	−0.85 ± 0.27
2.20000	1094 ± 861	−0.14 ± 0.57	11999 ± 0	−0.91 ± 0.42
3.64000	1726 ± 683	+0.10 ± 0.22	11999 ± 0	−1.28 ± 0.42
5.37000	1388 ± 1151	−0.39 ± 0.48	11999 ± 0	−0.92 ± 0.49
7.44000	1183 ± 1260	−0.47 ± 0.54	11999 ± 0	−0.92 ± 0.35
9.93000	3103 ± 998	−0.93 ± 0.15	11999 ± 0	−0.77 ± 0.40
		ID0918		
1.00000	2283 ± 2407	−1.01 ± 0.81	6360 ± 2312	−0.40 ± 0.81
2.20000	5744 ± 3858	−0.92 ± 0.92	8727 ± 4521	−0.95 ± 1.06
3.64000	4290 ± 2178	−0.81 ± 0.39	8655 ± 2772	−0.11 ± 0.53
5.37000	6454 ± 1810	−0.91 ± 0.71	10849 ± 3393	−0.51 ± 0.85
7.44000	2798 ± 3916	−0.27 ± 0.57	11961 ± 5520	−1.10 ± 0.65
9.93000	330 ± 898	−0.10 ± 0.13	6646 ± 2694	−0.67 ± 0.36
12.9100	499 ± 1566	−0.12 ± 0.28	9964 ± 2759	−0.79 ± 0.44

r (arcsec)	Age (young) (Myr)	*Z* (young) ($Z_\odot$)	Age (interm.) (Myr)	*Z* (interm.) ($Z_\odot$)	Age (old) Myr	*Z* (old) ($Z_\odot$)
			NGC 3073			
1.00000	81 ± 114	−0.15 ± 0.34	2398 ± 5246	−0.21 ± 0.88	13491 ± 6075	−1.93 ± 0.84
2.20000	375 ± 84	−0.02 ± 0.25	2865 ± 5447	−0.46 ± 0.90	11607 ± 6324	−1.72 ± 0.90
3.64000	379 ± 250	+0.22 ± 0.21	2225 ± 3114	−0.60 ± 0.53	17171 ± 3080	−2.20 ± 0.30
5.37000	443 ± 1257	+0.39 ± 0.24	1691 ± 1174	−0.62 ± 0.20	17826 ± 1636	−2.27 ± 0.26
7.44000	1098 ± 2877	−0.03 ± 0.37	1340 ± 554	−0.05 ± 0.18	17095 ± 2812	−1.84 ± 0.34
9.93000	742 ± 1985	+0.54 ± 0.28	1932 ± 1664	−0.44 ± 0.29	17308 ± 3029	−2.19 ± 0.45
12.9100	1515 ± 2985	+0.45 ± 0.33	2776 ± 2783	−0.10 ± 0.47	12316 ± 5707	−1.74 ± 0.57
16.4900	2194 ± 2750	+0.42 ± 0.37	3026 ± 3149	+0.33 ± 0.48	5991 ± 2572	−1.37 ± 0.29
20.7900	2188 ± 4513	+0.14 ± 0.32	9673 ± 5771	+0.04 ± 0.65	7691 ± 2440	−1.46 ± 0.70

This paper has been typeset from a TEX/LATEX file prepared by the author.